



Intracytoplasmic Trafficking of Nanoparticles based on Hyaluronic Acid and Chitosan for Targeted Delivery of Anticancer Drugs

Natalia Akentieva ^{1,*}, Artur Gizatullin ¹, Natalia Sanina ^{1,2}, Natalia Shkondina ¹, Kseniya Abramova ², Vladimir Tikhonov ³, Stanislav Shram ⁴, Sergey Aldoshin ^{1,2}

¹ Laboratory Biochemical and Cellular Studies, Department Kinetics of Chemical and Biological Processes, Institute of Problems of Chemical Physics Russian Academy of Sciences, Academician Semenov avenue 1, City Chernogolovka, Moscow Region 142432, Russia; na_aken@icp.ac.ru (N.A.);

² Lomonosov Moscow State University, Kolmogorova avenue 1, City Moscow 119991, Russia

³ Laboratory of Heterochain Polymers, Department of Macromolecular Compounds, Institute of Organoelement Compounds A.N. Nesmeyanov, Russian Academy of Sciences, st. Vavilova, 28, Moscow, 119334, Russia

⁴ Laboratory of Molecular Pharmacology of Peptides, Institute of Molecular Genetics of National Research Center Kurchatov Institute, Kurchatov Sq. 2, Moscow 123182, Russia

* Correspondence: na_aken@icp.ac.ru (N.A.);

Scopus Author ID 56370037400

Received: 22.04.2022; Accepted: 10.06.2022; Published: 11.09.2022

Abstract: Cancer diseases are characterized by high incidence and mortality worldwide. The main problem in cancer therapy is the lack of specificity of anti-cancer drugs. Therefore, the development of new methods of targeted delivery of anti-cancer drugs is an urgent task in oncology. Nanoparticles from hyaluronic acid and chitosan (HA:CS) were obtained using ionotropic gelation technology. The size of the nanoparticles was investigated using dynamic light scattering. Nanoparticles were obtained of a size of 100-400 nm. A physical association method has been developed for encapsulating nanoparticles with doxorubicin, a well-known antitumor drug, and dinitrosyl iron complex (DNIC; donor of nitric oxide). Using the method of dynamic light scattering, the surface potential of nanoparticles was measured. It was found that the resulting nanoparticles (HA-DOX:CS) were stable and had a surface potential of -45.6 meV. Using the method of confocal and FLIM microscopy, the localization of nanoparticles in cancer cells was studied. These methods have shown that nanoparticles pass through the cytoplasmic membrane and are localized inside the cells. It was also shown that nanoparticles (HA:CS-Rhod) were localized in the cytoplasm of African green monkey renal epithelial cells. It was found that the incorporation of DNIC into the composition of nanoparticles significantly increased the stability of DNIC, while prolonging the formation time and increasing the yield of nitric oxide. Thus, we have developed unique nanoparticles for the targeted delivery of antitumor drugs into cells.

Keywords: hyaluronic acid-chitosan nanoparticles; dinitrosyl iron complexes; cancer

© 2022 by the authors. This article is an open-access article distributed under the terms and conditions of the Creative Commons Attribution (CC BY) license (<https://creativecommons.org/licenses/by/4.0/>).

1. Introduction

Currently, oncological diseases are in second place (after cardiovascular diseases) in incidence and mortality worldwide. In particular, according to statistics, it was found that cancer accounted for almost 10 million deaths in 2020 [1]. The most common types of cancer are breast, lung, colon, rectum, and prostate.

The relevance of developing nanoparticles for targeted delivery of anti-cancer drugs is determined by the high frequency of oncological diseases worldwide, the low survival rate of

cancer patients, and the expensive treatment of cancer. Currently, the main problem in oncology is the lack of specificity in the action of many antitumor drugs [2]. Therefore, the main goal of cancer research is to develop treatments that cause the selective death of tumor cells. Currently, the main cancer treatment methods are surgery, radiotherapy, and chemotherapy. However, these approaches have a number of limitations. Surgical intervention and radiotherapy are often used already in the last stages of cancer development; these methods are not specific, and they do not suppress the formation of metastases [3]. Radiotherapy causes damage to normal cells and is accompanied by side effects [4]. Chemotherapeutic methods also have a number of disadvantages [5]. Currently, chemotherapy drugs are based on the rapid division of cancer cells and do not consider other specific properties of tumor cells. Therefore, most of the anti-cancer drugs used are non-specific-targeted. In addition, many drugs are highly toxic, show side effects, and have poor solubility, cell permeability, and biocompatibility [6]. Many chemotherapy drugs kill cancer cells and normal, healthy cells in the body [7]. Therefore, these drugs are highly toxic, such as platinum therapy [8]. In addition, these drugs kill normal healthy cells that divide rapidly, and conversely, slow-growing or dormant cancer cells remain alive. Thus, the lack of targeted, specific therapy for many types of cancer creates a need to develop new technologies (nanoparticles) that provide targeted delivery of drugs to cancer cells.

We have previously developed a method for obtaining nanoparticles of optimal size from hyaluronic acid and chitosan [9, 10]. However, the surface potential and localization of nanoparticles in the cell have not been studied. Therefore, this work aimed to study the surface potential of nanoparticles by dynamic light scattering and to study the localization of nanoparticles in tumor cells and renal epithelial cells using various methods. In addition, this study aimed to encapsulate the dinitrosyl iron complex (DNIC) in nanoparticles to increase the stability and effectiveness of their action.

2. Materials and Methods

2.1. Materials.

Commercial grade chitosan (M.w. = 100.000-300.000) manufactured by Acros Organics (New Jersey, USA) was used. HA (sodium hyaluronate, low molecular weight <0.1 MDa) was obtained from My formula (Germany), HyClone Fetal Clone III Serum was bought from GE Healthcare (USA), doxorubicin (DOX) was purchased from Ebeve Pharma (Austria). Sulforhodamine acid chloride (SRB) was purchased from Fluka (USA).

2.2. Cell lines.

The African green monkey renal epithelial cells (line *Vero*) were purchased from the Russian Collection of Vertebrate Cell Cultures (BioloT, St. Petersburg, Russia). The *HeLa* cell culture was obtained from ECACC (European Collection of Authenticated Cell Cultures, UK).

2.3. Cell culture.

The culture of HeLa cells (human cervix epitheloid carcinoma) is maintained in tissue culture flasks T-75 at 37⁰C in a 5% CO₂ atmosphere and culture with MEM cell medium supplemented with 10 % v/v HyClone Fetal Clone III Serum and 1 % v/v penicillin/streptomycin solution.

Vero cells were cultured in DMEM medium containing HEPES (10 mM, pH 7.2) supplemented with 10% fetal bovine serum (FBS), glutamine (0.15%), and gentamicin (50 mg/mL). The cell culture was incubated in an atmosphere of 5% CO₂ at 37°C and 90% humidity.

2.4. Fabrication of nanoparticles.

Nanoparticles (HA:CS), (HA-DNIC:CS), (HA-DOX:CS) were obtained by ion gelation [11]. Briefly, a portion of chitosan (10 mg, Mol.wt. = 100.000-300.000, Acros organics, USA) was dissolved in 1 ml of HCl (0.01 M, pH=2) and stirred for 12 hours. A portion of HA (40 mg, Mol.wt <0.1 MDa, My formula, Germany) was dissolved in 1 ml of distilled water and stirred for 12 hours. Then the resulting solutions of HA and chitosan were mixed in the ratio (HA:CS=4:1), and the pH of the solution was adjusted to pH=6.8 with phosphate buffer (2 ml, 0.1 M, pH=6.8) and stirred on a magnetic stirrer for 36 hours.

To study the localization of nanoparticles, nanoparticles (HA-DOX:CS){6:1} were prepared. A solution of doxorubicin (DOX) was added to a solution of chitosan, then a solution of hyaluronic acid was added in the ratio (HA:CS=6:1), and the pH of the solution was adjusted to pH=6.8 with phosphate buffer (2 ml, 0.1 M, pH=6.8).

2.5. Preparation of Lissamine Rhodamine B labeled chitosan (LRB-labeled chitosan).

The parent commercial chitosan was hydrolyzed, and its weight average molecular weight (M_w), molecular polydispersity (PD), and degree of acetylation (DA, %) were determined following the protocol and methods published in [12]. Prepared chitosan hydrochloride ($M_w = 6.7$ kDa, DP=2.6, DA=1%) taken in the amount of 1 g was dissolved in 50 mL water. The solution pH was adjusted to pH 6.3 and diluted with 25 mL methanol. After adding 0.025 g Sulforhodamine B acid chloride, the solution was stirred at 25°C for 24 hours. Then 5 mL concentrated ammonium hydroxide solution was added, and the resultant mixture was dialyzed against Milli-Q water. After the addition of 1 mL concentrated hydrochloric acid, the blue solution was lyophilized, and the product was dried over solid P₂O₅. The yield was 0.95 g. The degree of labeling was found to be 1 mol % using the extinction coefficient $\epsilon = 9.5 \cdot 10^4 \text{ M}^{-1} \cdot \text{cm}^{-1}$. Molecular characteristics of SRB-labeled chitosan hydrochloride ($M_w = 6.5$ kDa, DA=1%, PD=2.5) were determined, as it is shown above.

2.6. Preparation of hyaluronic acid-chitosan nanoparticles labeled with rhodamine (HA:CS-Rhod).

Hyaluronic acid-chitosan nanoparticles labeled with rhodamine (HA:CS-Rhod) were obtained by ionic gelation [11]. A portion of SRB-labeled chitosan (2.2 mg) was dissolved in 1 ml of HCl (0.2 M, pH = 2) and stirred for 12 hours. A portion of HA (40 mg, Mol.wt <0.1 MDa, My formula, Germany) was dissolved in 1 ml of distilled water and stirred for 12 hours. Then the resulting solutions of chitosan-rhodamine and HA were mixed in the ratio (HA:CS=4:1), the pH of the solution was adjusted to pH = 6.8 using phosphate buffer (2 mL, 0.1 M, pH = 6.8) and stirred on a magnetic stirrer for 36 hours.

2.7. Analysis of size and potential zeta nanoparticles by dynamic light scattering (DLS).

Nanoparticles (HA:CS; HA-DOX:CS) size distribution was studied using a DLS technique (Nanopartica SZ-100; HORIBA Ltd, Kyoto, Japan). The scattered light from the

particles present in the sample was collected either at 90 or 173 degrees, automatically selected by the instrument as the optimum scattering angle based on sample concentration. The zeta potential (mV), which is an indicator of dispersion and stability of the prepared nanoparticles (HA:CS; HA-DOX:CS), was measured according to the method [13].

2.8. Synthesis of the dinitrosyl iron complex (DNIC).

Synthesis and identification of the DNIC#6 compound were carried out according to the procedure [14] as the tested compound used a synthetic analog of mononuclear dinitrosyl iron complex with functional sulfur-containing ligands, namely with thiourea and its derivatives $[\text{Fe}(\text{SC}(\text{NH}_2)_2)_2(\text{NO})_2]\text{ClO}_4\text{Cl}$ (DNIC#6). The structures of DNIC#6 have been confirmed by X-ray analysis, Mössbauer, IR, and EPR spectroscopy [14-18]; when dissolved in water solvents, these DNIC#6 released NO as a result of complex dissociation [14].

2.9. Analysis localization of nanoparticles (HA-DOX:CS) with confocal microscopy.

The cells were imaged with an inverted laser scanning confocal microscope (LSCM) LSM780 (Zeiss, Germany), excitation by a 488 nm laser and a fluorescence emission range from 550 nm to 700 nm. Fluorescence z-stack projections were obtained and analyzed with the ZEN2010 software [19].

2.10. Analysis of localization of nanoparticles (HA-DOX:CS) by Fluorescent Life Imaging Microscopy.

FLIM was performed as described previously [20]. The setup was developed on an inverted RM21 (MadCityLabs) equipped with a Nikon CFI plan APO 100× oil immersion objective (NA: 1.45, 0.17 WD 0.13) and an avalanche photodiode detector (PD50CTD, MPD). The source of laser excitation was a picosecond pulsed laser with a wavelength of 467 nm (PLP 10, pulse duration 80 ps, repetition rate 20 MHz, Hamamatsu), used with a cleaning filter to ensure the monochromaticity of the laser source, a spatial filter, a planar filter, concave lenses for beam expansion, dichroic to reflect lasers to the rear entrance of the objective and collect the fluorescent signal emitted by the sample. In addition, a long transmission filter was installed in the detection path in front of the detector to remove some scattered laser background and a lens that focuses the signal to the detection area of 50 μm APD. Micro- and nano-positioning (MCL) steps were used to control sample deposition. Time-Correlated Single Photon Counting (TCSPC) was performed using a single photon counting board (SPC130, Becker & Hickl).

2.11. Analysis of localization nanoparticles (HA:CS-Rhod) by confocal microscopy.

Vero cells were seeded on 0.17 μm glass coverslips (12 × 12 mm) in cell culture on 24 well plates at a density of 30,000 cells/well and grown for 24 hours in a CO₂ incubator. After that, the growth medium was removed, and the mixture of fresh growth medium (100 μL) and nanoparticles (HA:CS-Rhod, 20 μL) was added to the cells. Then the mixture was incubated at 37°C for 30 min in a CO₂ incubator. After incubation, the growth medium was removed, and the cells were washed twice with phosphate-buffered saline (PBS, pH 7.6) and fixed in 3.7% formaldehyde in PBS (250 μL/well) for 30 min at room temperature. The samples were then washed twice with PBS, containing 2% BSA and 0.25% Triton X-100. After that, the samples were washed three times with PBS and stained with FITC-phalloidin (0.25 μmol) to visualize the actin cytoskeleton. Samples were incubated for 1 hour at room temperature in the dark.

Then the FITC-phalloidin solution was aspirated, the cells were washed three times with PBS, and the glass coverslips were removed, mounted by Fluoro-gel 11 with DAPI, and placed on glass slides. Microfluorescence analysis of DAPI, FITC, and rhodamine was performed on an LSM510M microscope (Zeiss, Germany) using Plan-Neofluar 40x/1,3 Oil Dic objective and lasers emitting at 404, 488, and 543 nm.

2.12. Electrochemical determination of NO concentration, isolated from DNIC.

To measure the concentration of NO generated from DNIC, an amperometric sensor electrode "amiNO-700" of the "inNO Nitric Oxide Measuring System" system (Innovative Instruments, Inc., USA) was used. The NO concentration in the aqueous solution was recorded for ~500 seconds (with a step of 0.2 seconds). The sensor electrode was calibrated using a standard aqueous solution of NaNO₂ (100 μM), to which a mixture of aqueous solutions of KI (0.12 M, 18 mL) and H₂SO₄ (1 M, 2 mL) was added [21]. To analyze NO released from DNIC, a weighed portion of DNIC was prepared and dissolved in water to a final concentration of 4x10⁻⁴M. Then the prepared solution was stirred on a magnetic stirrer at room temperature for 1 and 10 min. After that, aliquots (0.5 ml) of the DNIC solution were placed into the measuring electrochemical cell. Then 49.5 ml of buffer (Buffers, HydrionR Chemvelope Sygma-Aldrich, USA, pH=7.0) was added to the cell, and the temperature sensor and electrode were immersed in it. The release of NO was recorded in the system for 500 seconds (~8.3 min) at a temperature of 25°C.

2.13. Electrochemical determination of the amount of nitric oxide released from iron dinitrosyl complex in the composition of chitosan-hyaluronic acid nanoparticles.

To analyze the NO-donor activity (HA-DNIC#6:CS), a solution of DNIC#6 with nanoparticles (DNIC#6 concentration 4x10⁻⁴M) was prepared in the following way. A solution of 1 ml of nanoparticles (HA:CS=4:1) was added to a weighed portion of DNIC#6 and stirred on a stirrer for 5, 10, 20, 40, and 60 min. Then, a solution of distilled water (9 ml) was added to the 1 ml solution of DNIC, mixed. Afterward, aliquots of 0.5 ml of the complex solution were taken and transferred to a measuring electrochemical cell, to which 49.5 ml of buffer, pH = 7, was added beforehand. Then the amount of NO released from nanoparticles (HA-DNIC#6:CS) was recorded for 500 sec at a temperature of 25°C.

3. Results and Discussion

3.1. Determination of size and surface zeta potential of nanoparticles by dynamic light scattering.

Nanoparticles (HA:CS) were obtained using the method of physical association due to ion self-assembly of hyaluronic acid molecules (negatively charged) and chitosan molecules (positively charged) in nanogels, as described earlier [9, 10, 12]. The obtained nanoparticles were water soluble due to the hydrophilicity of HA and chitosan. Physical association performed the encapsulation of DOX in nanoparticles (HA-DOX:CS). Then the surface potential of the nanoparticles was investigated by the dynamic light scattering method (Table 1).

Table 1. Surface zeta potential of nanoparticles.

#	Nanoparticle preparation methods	Surface zeta potential meV
1	Nanoparticles (HA:CS) {4:1}	-1.74 meV
2	(HA-DOX: CS) {4:1}	-2.3 meV
3	(HA-DOX :CS) {6:1} stirred 10 min	-6.16 meV
4	(HA-DOX :CS) {12:1} stirred 30 min	-7.06 meV
5	(HA-DOX:CS) {12:1} stirred 30 min + ultrasound	-8.1 meV
After washing and ultrasound treatment		
6	Nanoparticles (HA:CS) {4:1}	-47.22 meV
7	(HA-DOX:CS) {6:1} stirred 10 min	-45.6 meV
8	(HA-DOX:CS) {12:1} stirred 30 min	-39.4 meV

It was shown that nanoparticles (HA:CS){4:1} had a potential of -47.22 meV, and nanoparticles (HA-DOX:CS){6:1} had a potential of -45.6 meV. This indicates that the nanoparticles are negatively charged and stable.

The hydrodynamic radius of the nanoparticles (HA:CS){4:1} was determined using the dynamic light scattering method (Figure 1).

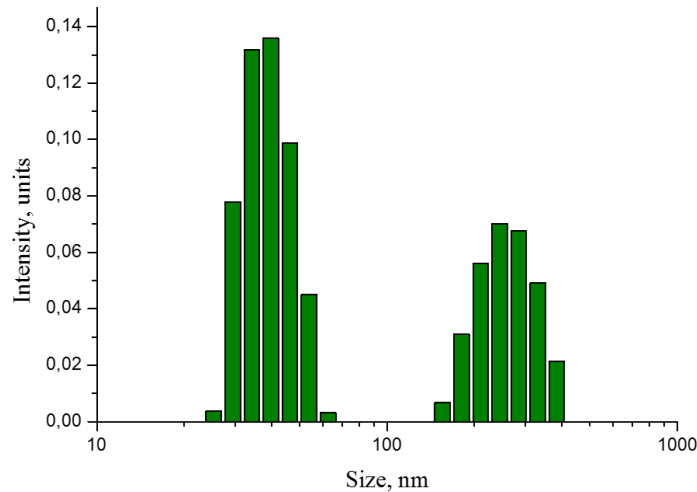


Figure 1. Determination of the hydrodynamic radius of nanoparticles (HA:CS){4:1} by dynamic light scattering.

The results of measurements by the DLS method showed that the nanoparticle size (HA:CS) {4:1} was in the range of 30–60 and 100–400 nm.

The results showed that the nanoparticles (HA-DOX:CS)){6:1} were 100 ~ 300 nm in size (Figure 2). The results of Figure 1 and Figure 2 showed a polydisperse distribution with at least two nanoparticle populations.

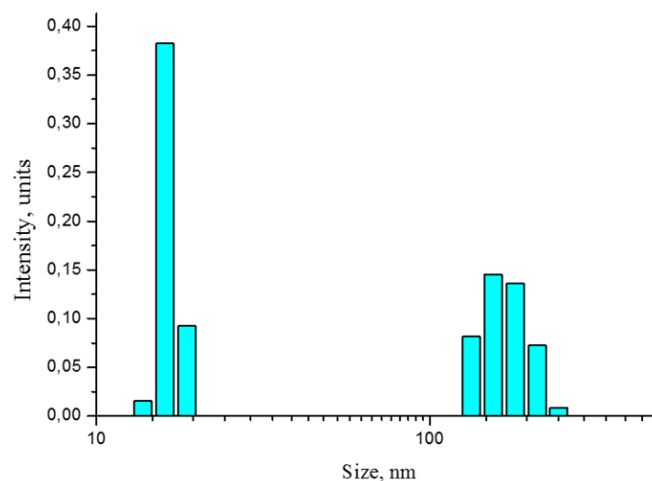


Figure 2. Determination of the size of nanoparticles (HA-DOX: CS){6:1} by dynamic light scattering.

Thus, using different ratios of chitosan and HA, a method was developed for producing nanoparticles of various sizes with encapsulated DOX. The optimal nanoparticle size (100 nm) was obtained with the ratio HA:CS = 6:1.

3.2. Determination of localization of nanoparticles in cells.

To study the localization of nanoparticles, nanoparticles with doxorubicin (HA-DOX:CS) {6:1} were prepared. Doxorubicin has its fluorescence $E_{ex}/E_{em} = 470/595$ nm, making it possible to use it to visualize nanoparticles in a cell [22, 23].

The penetration of nanoparticles (HA-DOX:CS) into HeLa cells was studied by conventional and FLIM confocal microscopy.

Confocal microscopy showed that nanoparticles (HA-DOX:CS) pass through the cytoplasmic membrane of cells and are localized in the cytoplasm of HeLa cells (Figure 3, yellow fluorescence).

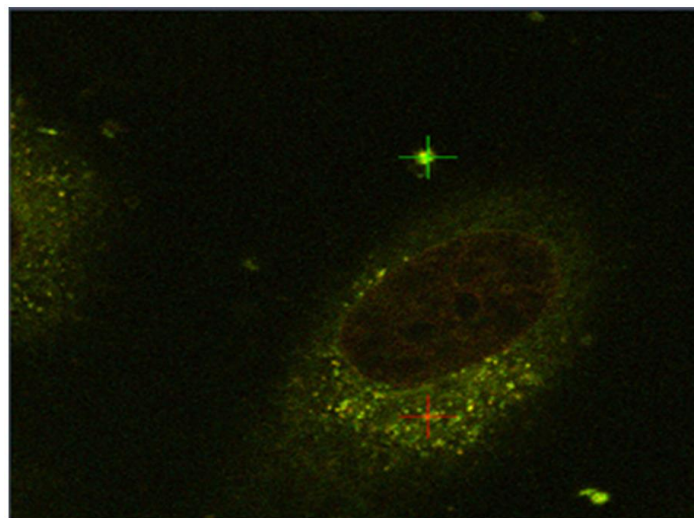


Figure 3. Localization of nanoparticles (HA-DOX:CS) in *HeLa* cells: the confocal image of *HeLa* cells after incubation with nanoparticles (HA-DOX:CS) for 24 hours (yellow fluorescence); the emission signal of the trackers (green, red fluorescence). Objective 40 \times .

The results of the analysis of the localization of nanoparticles in living cells using FLIM microscopy showed that free DOX accumulates in the nucleus of HeLa cells after 24 hours of incubation (Figure 4, bottom panel). It was found that nanoparticles (HA-DOX: CS) were localized inside the cells after incubation with HeLa cells for 24 hours (Figure 4, upper panel).

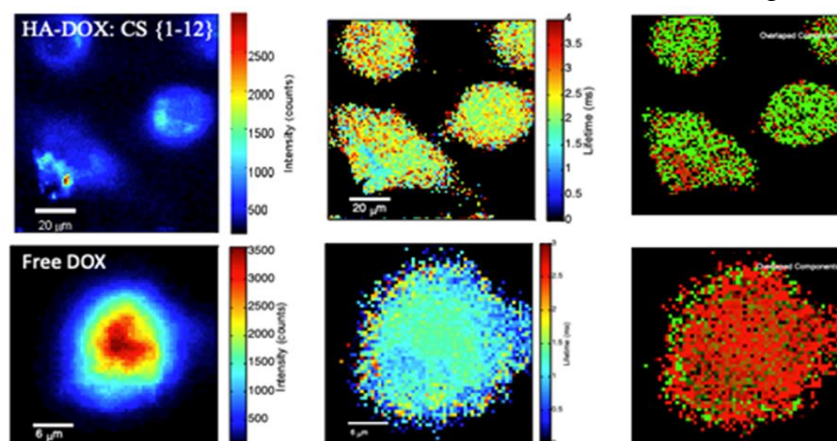


Figure 4. Localization of nanoparticles (HA-DOX:CS) in *HeLa* cells. FLIM images of live *HeLa* cells incubated with nanoparticles (HA-DOX:CS) (upper panel) and with free doxorubicin (lower panel) for 24 hours.

Thus, both methods confirmed the passage of nanoparticles through the cytoplasmic membrane of cells and showed the localization of nanoparticles in the cytoplasm and around the nucleus after 24 hours of incubation.

3.3. Study of the localization of nanoparticles (HA:CS-Rhod) in Vero cells.

To study the ability of nanoparticles to penetrate into the cell and their localization, nanoparticles were prepared from hyaluronic acid and chitosan labeled with rhodamine (HA:CS-Rhod){4:1}, as described in "Methods of research".

The results showed that nanoparticles (HA:CS-Rhod) were also localized in the cytoplasm of green monkey *Vero* epithelial cells (Figure 5).

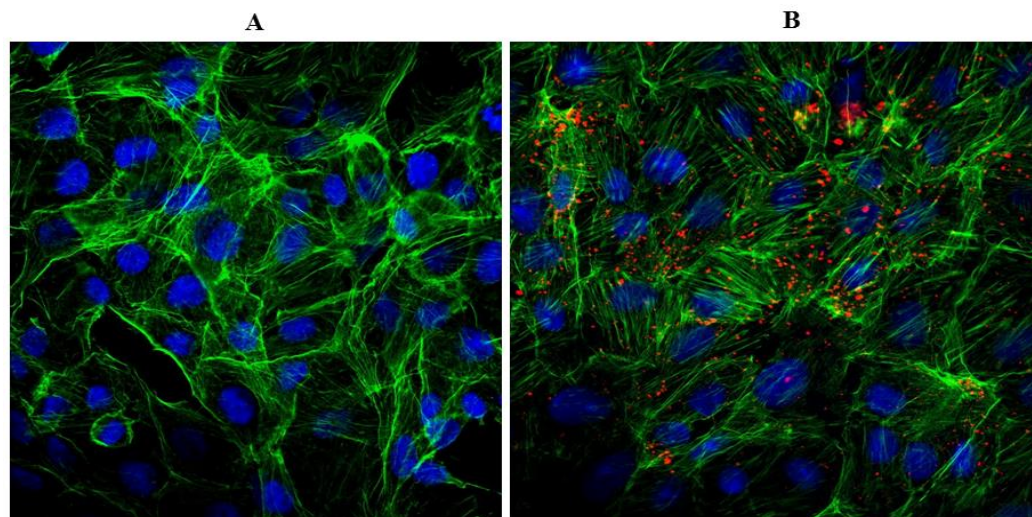


Figure 5. Localization of nanoparticles (HA:CS-Rhod) in cells: (A) *Vero* cells, control; (B) *Vero* cells, incubated with nanoparticles (HA:CS-Rhod). Cell nucleus stained with DAPI (blue fluorescence), cell actin stained with FITC-phalloidin (green fluorescence), and chitosan labeled with rhodamine (red fluorescence). Objective 40x. Images size – 232.5 μm x 232.5 μm .

Presently, in oncology, for cancer treatment, decreases are used drugs that are donors of nitric oxide [24-27]. However, the main problem with these drugs is that these drugs are often unstable, nonspecific, and have a number of side effects. Therefore, the development of nanoparticles for stabilization and targeted delivery of DNICs drugs is currently relevant.

The encapsulation of DNIC#6 in nanoparticles was carried out by ion gelatinization. Then we investigated the release of NO from DNIC#6 in an aqueous solution and in the composition of nanoparticles (HA-DNIC#6:CS) (Figure 6).

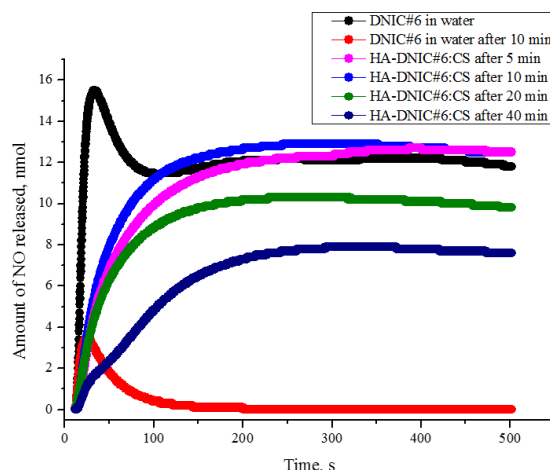


Figure 6. Generation of NO from the DNIC#6 and from nanoparticles (HA-DNIC#6:CS).

It was found that upon dissolution of DNIC in an aqueous solution, a dramatic drop in generation NO is observed (compare curves ● and ● on Figure 6), and in the 100 seconds of detection, the level of generated NO drops to almost zero (Figure 6, curve ●). This indicated that the DNIC complex quickly decomposes in water and ceases to emit NO. Next, we analyzed the release of NO from the nanoparticles (HA-DNIC#6:CS). It was shown that after the addition of DNIC#6 to the nanoparticles, 13 nmol NO is released, and this level remains stable for a long time (> 500 seconds) (Figure 6, curves ● and ●). The solution of DNIC#6 in the composition of nanoparticles continues to release nitric oxide (10 nmol) stably even after 20 min (Figure 6, curve ●). Even after 40 min, the DNIC#6 solution in the composition of nanoparticles releases about 8 nmol of nitric oxide, and the generation of nitric oxide remains at the same level (Figure #6, curve ●). These data indicate that a significant stabilization of the DNIC#6 complex is observed in the composition of nanoparticles, which leads to a prolonged release of nitric oxide with a high yield.

4. Conclusions

In this work, we prepared multilayer nanoparticles consisting of a chitosan biopolymer carrier and a hyaluronic acid delivery vector, and then doxorubicin or DNIC was encapsulated into these nanoparticles. We assume that the specificity of the action of these nanoparticles (hyaluronic acid-chitosan) will be carried out using three types of targeting: tissue, cellular and molecular.

Tissue targeting will be carried out due to the fact that we have developed a method for obtaining nanoparticles of a special size (100–400 nm), with a surface layer in the form of hyaluronic acid, which will allow nanoparticles to selectively bind to tumor tissue and increase the circulation time of nanoparticles in the blood vessels of tumors. As a carrier in nanoparticles, we used chitosan, an amino sugar, a derivative of a linear polysaccharide whose macromolecules consist of randomly linked β -D-glucosamine units and N-acetyl-D-glucosamine [28]. Chitosan is a highly cationic, non-toxic, biocompatible, and biodegradable compound [29]. Due to its cationic nature, chitosan is able to form insoluble complexes with the anionic polysaccharide hyaluronic acid. This ability allows it to be used as a carrier in nanoparticles. These chitosan-based nanoparticles are able to perform the necessary function in the human body for a long time and then decompose and are excreted from the body without causing harm to a person [30, 31].

The cell-targeting strategy makes it possible to deliver drugs directly to tumor cells, rather than being concentrated in the kidneys and liver and then excreted from the body by the reticuloendothelial system. To this end, to increase the targeted efficiency of nanoparticles, we used the concept of active targeted delivery, which consists of the biomolecular recognition of molecules on the cell surface, leading to a higher degree of specificity. In this case, we decorated the nanoparticles with a biologically targeted molecule. As such a molecule, we used HA, the main component of the extracellular matrix in the bone marrow, connective, epithelial, and nervous tissues [32, 33]. HA is a non-sulfonated glycosaminoglycan, a negatively charged polymer that is biocompatible, non-toxic, and readily biodegradable [34]. In addition, HA can protect the delivered drug and improve the solubility of hydrophobic drugs. This biopolymer regulates various cellular processes, including proliferation, differentiation, motility, invasiveness, cell adhesion, and gene expression in cancer cells [35-38]. HA is a physiological ligand for CD44 and RHAMM receptors. Therefore, HA will specifically interact with CD44 and RHAMM receptors on the surface of the tumor cell membrane, providing selective delivery

of the drug into the cell [39-42]. Hyaluron-binding receptors (CD44 and RHAMM) are promising targets for developing a new generation of HA nanoparticles [43, 44]. It is now known that CD44 and RHAMM receptors are synthesized in excess in aggressive cancer cells such as breast cancer, prostate cancer, solid tumors, blood cancer, myeloid leukemia, multiple myeloma, and a number of others [45-47]. At the same time, this receptor is contained in insignificant amounts in normal cells. Therefore, HA-based nanoparticles will increase the efficiency of targeted drug delivery and accelerate their intracellular delivery due to endocytosis since all cells express endogenous receptors for this polymer (CD44 and RHAMM receptors) [48]. In addition, HA has a negative charge, which ensures the rapid passage of nanoparticles through the cytoplasmic membrane, which is also negatively charged [49]. By selecting different ratios of chitosan and HA, we obtained nanoparticles with a negative surface charge (-47.22 meV and -45.6 meV). Such nanoparticles will be able to more easily penetrate cancer cells since the membranes of tumor cells have a more negative charge than normal cells [50]. This will provide additional selectivity for drug delivery to cancer cells. It is known that overexpression of the CD44 receptor is observed in macrophages and HeLa tumor cells [51]. Previously, various methods have been developed to analyze the intracellular localization of nanoparticles and changes in physical parameters inside the cell [52, 53]. In particular, we developed a GFP-based manometry method to analyze temperature changes induced by a chemical reagent that allows one to distinguish between local heating variations within different cellular compartments [52].

In addition, the multi-photon fluorescence lifetime imaging microscopy (MP-FLIM) method was developed to evaluate the delivery systems of anti-cancer drugs [53]. In particular, MP-FLIM has been used to monitor the therapeutic effect of elesclomol, an anti-cancer drug, to track NAD(P)H cofactors with sub-cellular resolution on live cells exposed to an anti-cancer nanocarrier [53].

In our work, using confocal and FLIM microscopy, we showed that the nanoparticles obtained by us pass through the cytoplasmic membrane and are localized inside *HeLa* cancer cells and inside *Vero* cells. Additionally, cellular enzymes (hyaluronidases) are able to break down HA inside the cell, thereby releasing the drug directly into the cancer cell [54]. This strategy allows specific, cell-targeted delivery of anti-cancer drugs. Polysaccharide-coated nanoparticles are a new trend in drug delivery systems. Active targeted delivery of drugs associated with HA is a promising approach in biomedicine.

We believe that the nanoparticles obtained by us will also act through molecular targeting, the essence of which is the encapsulation of highly effective drugs into nanoparticles that purposefully affect the molecular target inside the cancer cell. Such particles can also carry and deliver various drugs with antitumor activity (for example, doxorubicin, paclitaxel, etc.) into the cell. In this work, we encapsulated doxorubicin, a well-known antitumor drug [55], into nanoparticles and showed by confocal and FLIM microscopy that these nanoparticles penetrate tumor cells and localize in the cytoplasm. Thus, the nanoparticles we obtained can deliver anti-cancer drugs directly to cancer cells. In addition, enzyme inhibitors/activators (matrix metalloproteinase, histone deacetylase, myeloperoxidase, polyadenine ribose polymerase, etc.) can be used as drugs.

It should be noted that compounds that are donors of nitric oxide (NO) are currently used in oncology to treat oncological diseases [56-64]. Diazenium diolates, which are direct NO donors, are known to regulate the activity of endothelial nitric oxide synthase [65, 66]. These compounds exhibit antitumor activity against lung, liver, and breast cancer [66, 67].

However, the main problem with these drugs is that they are poorly soluble and unstable in water, nonspecific, and have a number of side effects [68, 69].

We have previously shown that DNICs are effective inhibitors of such enzymes as myeloperoxidase, renin, matrix metalloproteinase, and poly(ADP-ribose) polymerase [70-72]. DNICs are synthetic analogs of natural highly reactive nitrosyl cellular intermediates formed *in vivo* in reactions of endogenous NO with active centers of non-heme proteins and demonstrate high biological (including antitumor) activity [68-74]. The stabilization and targeted delivery of DNIC is a very urgent task. In our work, we encapsulated DNIC into nanoparticles and studied the stability of DNIC and the generation of nitric oxide over time. Our study showed that the encapsulation of DNIC in the composition of nanoparticles significantly increases the stability of this compound, prolongs the generation of NO, and increases the yield of nitric oxide, thereby probably increasing the effectiveness of this compound.

Thus, we have shown that the nanoparticles we created are capable of tissue, cellular, and molecular targeting to ensure the specificity of the action of anti-cancer drugs. Such nanoparticles, which deliver targeted drugs directly to a cancer cell, will qualitatively and effectively improve the treatment of oncological diseases. Currently, there are many publications on the creation of inorganic and organic nanoparticles to deliver anti-cancer drugs. Examples of inorganic nanoparticles include gold nanoparticles, magnetic iron oxide, quantum dots, and carbon nanotubes [75, 76]. In addition, nanoparticles are based on organic materials, such as polymer nanoparticles, nanogels, and peptide nanoparticles [77, 78]. The undoubted advantage of our nanoparticles is that we use the natural biopolymer chitosan as a nanostructural material, which is a biocompatible and biodegradable material [28, 30]. It should be noted that the nanoparticles we obtained are water-soluble, biocompatible, biopermeable, and easily biodegradable, capable of releasing the drug inside the cell due to HA cleavage by hyaluronidases.

Such nanoparticles will undoubtedly be of interest to the pharmaceutical industry since they are a combination of safe biomaterials, ideal for encapsulating cationic hydrophilic drugs, able to provide intracellular drug delivery, and can perform the necessary drug delivery function for a long time without causing adverse side effects for the human body, can be produced simply and easily on a large scale in nanotechnology, and finally are stable. However, further studies of these nanoparticles in animal models *in vivo* are needed.

Funding

This research was funded by the Ministry of Science and Higher Education of the Russian Federation and performed under the state task, state registration # AAAA-A19-119071890015-6.

Acknowledgments

The authors would like to express their gratitude to the REC MGOU "Medical Chemistry" at the IPCP RAS (Chernogolovka, Moscow area, Russia), and the Center of Cellular and Genomic Technologies of the Institute of Molecular Genetics of National Research Center "Kurchatov Institute" (Moscow, Russia) for supporting this study. This work benefitted from the scientific visitor programme of the INL – International Iberian Nanotechnology Laboratory, headquarters in Braga, Portugal, which provided access and support to customers and

commercial setups associated with Nanophotonics and Bioimaging research core facilities (DLS, confocal microscopy) and the Ultrafast Bio- and Nanophotonics group (FLIM microscopy) to visiting researcher Artur Gizatullin under the local supervision of Jana B. Nieder. Oscar Silvestre (INL) is kindly acknowledged for help with the nanoparticle characterization and confocal microscopy, and Oleksandr A. Savchuk (INL) for his support of the FLIM microscope

Conflicts of Interest

The authors declare no conflict of interest. The funders had no role in the study's design, in the collection, analyses, or interpretation of data, in the writing of the manuscript, or in the decision to publish the results.

References

1. WHO. *International Agency for Research on Cancer* **2020**, press release 292, 1-3.
2. Suvarna, C.; Chaitanya, N.C.; Ameer, S.; Inamdar, P.; Alugubelli, S.; Bhagyanagar, A. Chemopreventive Agents in Oral Premalignancy: A Medical Management Review. *J Int Soc Prev Community Dent* **2020**, *10*, 127-133, https://doi.org/10.4103%2Fjispd.JISPCD_424_19.
3. Martín-Pérez, B.; Dar, R.; Bislenghi, G.; Stijns, J.; Grégoir, T.; Wolthuis, A.M.; D'Hoore, A. Transanal Minimally Invasive Proctectomy With Two-Stage Turnbull-Cutait Pull-Through Coloanal Anastomosis for Iatrogenic Rectourethral Fistulas. *Dis Colon Rectum* **2021**, *64*, e26-e29, <https://doi.org/10.1097/dcr.0000000000001850>.
4. Ge, D.; Zou, X.; Chu, Y.; Zhou, J.; Xu, W.; Liu, Y.; Zhang, Q.; Lu, Y.; Xia, L.; Li, A.; Huang, C.; Wang, P.; Shen, C.; Chu, Y. Analysis of volatile organic compounds in exhaled breath after radiotherapy. *J Zhejiang Univ Sci B* **2022**, *23*, 153-157, <https://doi.org/10.1631%2Fjzus.B2100447>.
5. Dreţcanu, G.; Iuhas, C.I.; Diaconeasa, Z. The Involvement of Natural Polyphenols in the Chemoprevention of Cervical Cancer. *Int J Mol Sci* **2021**, *22*, 8812, <https://doi.org/10.3390/ijms22168812>.
6. Lin, A.; Giuliano, C.J.; Palladino, A.; John, K.M.; Abramowicz, C.; Yuan, M.L.; Sausville, E.L.; Lukow, D.A.; Liu, L.; Chait, A.R.; Galluzzo, Z.C.; Tucker, C.; Sheltzer, J.M. Off-target toxicity is a common mechanism of action of cancer drugs undergoing clinical trials. *Sci Transl Med* **2019**, *11*, eaaw8412, <https://doi.org/10.1126/scitranslmed.aaw8412>.
7. Anderson, J.T., Huang, K.M., Lustberg, M.B., Sparreboom, A., Hu, S. Solute Carrier Transportome in Chemotherapy-Induced Adverse Drug Reactions. In: Stock, C., Pardo, L.A. (eds) *Targets of Cancer Diagnosis and Treatment. Reviews of Physiology, Biochemistry and Pharmacology* **2020**, *183*, Springer, Cham, https://doi.org/10.1007/112_2020_30.
8. Guan, L.Y.; Lu, Y. New developments in molecular targeted therapy of ovarian cancer. *Discov Med* **2018**, *26*, 219-229.
9. Gizatullin, A.R.; Akentieva, N.P.; Sanina, N.A.; Dremova, N.N.; Torbov, V.I.; Shkondina, N.I.; Prichodchenko, T.R.; Aldoshin, S.M. Design nanoparticles (chitosan-hyaluronic acid) for target delivery of dinitrosyl iron complexes, potential cardiac drugs. *Butlerov's communications* **2018**, *54*, 138-143.
10. Akentieva, N.P.; Gizatullin, A.R.; Sanina, N.A.; Dremova, N.N.; Torbov, V.I.; Shkondina N.I.; Zhelev, N.; Aldoshin, S.M. Fabrication of chitosan-hyaluronic acid nanoparticles and encapsulation into nanoparticles of dinitrosyl iron complexes as potential cardiological drugs. *Nanomedicine J* **2020**, *7*, 199-210, <https://doi.org/10.22038/nmj.2020.07.0004>.
11. Abolhasani, A.; Heidari, F.; Abolhasani, H. Development and characterization of chitosan nanoparticles containing an indanonic tricyclic spiroisoxazoline derivative using ion-gelation method: an in vitro study. *Drug Dev Ind Pharm* **2020**, *46*, 1604-1612, <https://doi.org/10.1080/03639045.2020.1811304>.
12. Berezin, B.B.; Bezrodnykh, E.A.; Blagodatskikh, I.V.; Yamskov, I.A.; Tikhonov, V.E. Extraction of residual heavy metals from commercial chitosan and approach to oligochitosan hydrochloride. *Carbohydr Polym* **2019**, *215*, 316-321, <https://doi.org/10.1016/j.carbpol.2019.03.072>.
13. Pasupuleti, V.R.; Prasad, T.N.; Sheikh, R.A.; Balam, S.K.; Narasimhulu, G.; Reddy, C.S.; Rahman, I.; Gan, S.H. Biogenic silver nanoparticles using *Rhinacanthus nasutus* leaf extract: synthesis, spectral analysis, and antimicrobial studies. *Int. J. Nanomedicine* **2013**, *8*, 3355-3364, <https://doi.org/10.2147/ijn.s49000>.

14. Sanina, N.A.; Aldoshin, S.M.; Shmatko, N.Yu.; Korchagin, D.V.; Shilov, G.V.; Knyaz'kina, E.A.; Ovanesyan, N.S.; Kulikov, A.V. Nitrosyl iron complexes with enhanced NO releasing ability: synthesis, structure and properties of new type of salts with DNIC cations $[\text{Fe}(\text{SC}(\text{NH}_2)_2)_2(\text{NO})_2]^+$. *New J Chem* **2015**, *39*, 1022-1030, <https://doi.org/10.1039/C4NJ01693A>.
15. Sanina, N.A.; Aldoshin, S.M.; Shmatko, N.Yu.; Korchagin, D.V.; Shilov, G.V.; Ovanesyan, N.S.; Kulikov, A.V. Mesomeric tautomerism of ligand is a novel pathway for synthesis of cationic dinitrosyl iron complexes: X-ray structure and properties of nitrosyl complex with thiourea. *Inorg Chem Commun* **2014**, *49*, 44-47, <https://doi.org/10.1016/j.inoche.2014.09.016>.
16. Sanina, N.A.; Manzhos, R.A.; Emel'yanovaa, N.S.; Kupchinskaya, E.N.; Krivenko, A.G.; Aldoshin, S.M. Redox reactions of cationic nitrosyl iron complexes with thiourea and its aliphatic derivatives: The experiment and DFT investigation. *Journal of Molecular Structure* **2019**, *1181*, 253-260, <https://doi.org/10.1016/j.molstruc.2018.12.112>.
17. Shmatko, N.Yu.; Korchagin, D.V.; Shilov, G.V.; Ovanesyan, N.S.; Kulikov, A.V.; Sanina, N.A.; Aldoshin, S.M. The cationic dinitrosyl iron complexes family with thiocarbamide derivatives: Synthesis, structure and properties in the solid state. *Polyhedron* **2017**, *137*, 72-80, <https://doi.org/10.1016/j.poly.2017.08.006>.
18. Shmatko, N.Yu.; Korchagin, D.V.; Shilov, G.V.; Sanina, N.A.; Aldoshin S.M. Molecular and crystal structure of a cationic dinitrosyl iron complex with 1, 3-dimethylthiourea. *J Struct Chem* **2017**, *58*, 353-355, <https://doi.org/10.1134/S0022476617020172>.
19. Gonçalves Lopes, R.C.F.; Silvestre, O.F.; Faria, A.R.; C do Vale, M.L.; Marques, E.F.; Nieder, J.B. Surface charge tunable catanionic vesicles based on serine-derived surfactants as efficient nanocarriers for the delivery of the anti-cancer drug doxorubicin. *Nanoscale* **2019**, *11*, 5932-5941, <https://doi.org/10.1039/C8NR06346J>.
20. Figueiras, E.; Silvestre, O.F.; Ihalainen, T.O.; Nieder, J.B. Phasor-assisted nanoscopy reveals differences in the spatial organization of major nuclear lamina proteins. *Biochim Biophys Acta Mol Cell Res.* **2019**, *1866*, 118530, <https://doi.org/10.1016/j.bbamcr.2019.118530>.
21. Zhang X., Broderick M. Amperometric detection of nitric oxide. *Mod Asp Immunobiol* **2000**, *1*, 160-165.
22. Dong, X.; Yang, A.; Bai, Y.; Kong, D.; Lv, F. Dual fluorescence imaging-guided programmed delivery of doxorubicin and CpG nanoparticles to modulate tumor microenvironment for effective chemo-immunotherapy. *Biomaterials* **2020**, *230*, 119659, <https://doi.org/10.1016/j.biomaterials.2019.119659>.
23. Hayat, S.M.G.; Jaafari, M.R.; Hatamipour, M.; Penson, P.E.; Sahebkar, A. Liposome Circulation Time is Prolonged by CD47 Coating. *Protein Pept Lett* **2020**, *27*, 1029-1037, <https://doi.org/10.2174/0929866527666200413100120>.
24. Fan, L.; Zheng, N.; Peng, F.; Zhao, Z.; Fan, D.; Cai, S.; Tao, L.; Wang, Q. Nitric oxide affects cisplatin cytotoxicity oppositely in A2780 and A2780-CDDP cells via the connexin32/gap junction. *Cancer Sci* **2020**, *111*, 2779-2788, <https://doi.org/10.1111/cas.14436>.
25. Sinha, B.K.; Perera, L.; Cannon, R.E. NCX-4040, a Unique Nitric Oxide Donor, Induces Reversal of Drug-Resistance in Both ABCB1- and ABCG2-Expressing Multidrug Human Cancer Cells. *Cancers* **2021**, *13*, 1680, <https://doi.org/10.3390/cancers13071680>.
26. Klink, M.; Kielbik, M.; Kielbik, I.S.; Przygodzka, P.; Sulowska, Z. Antitumoral activity of nitric oxide-releasing compounds. *Redox Biol* **2015**, *5*, 420, <https://doi.org/10.1016/j.redox.2015.09.031>.
27. Bonavida, B. Sensitizing activities of nitric oxide donors for cancer resistance to anti-cancer therapeutic drugs. *Biochem Pharmacol* **2020**, *176*, 113913, <https://doi.org/10.1016/j.bcp.2020.113913>.
28. Bi, S.; Wang, M.; Huang, L.; Qin, D.; Cheng, X.; Chen, X. Evaluation of structure transformation and biocompatibility of chitosan in alkali/urea dissolution system for its large-scale application. *Int J Biol Macromol* **2020**, *154*, 758-764, <https://doi.org/10.1016/j.ijbiomac.2020.03.075>.
29. Abd El-Hack, M.E.; El-Saadony, M.T.; Shafi, M.E.; Zaberemawi, N.M.; Arif, M.; Batiha, G.E.; Khafaga, A.F.; Abd El-Hakim, Y.M.; Al-Sagheer, A.A. Antimicrobial and antioxidant properties of chitosan and its derivatives and their applications: A review. *Int J Biol Macromol* **2020**, *164*, 2726-2744, <https://doi.org/10.1016/j.ijbiomac.2020.08.153>.
30. Prasathkumar, M.; Sadhasivam, S. Chitosan/Hyaluronic acid/Alginate and an assorted polymers loaded with honey, plant, and marine compounds for progressive wound healing-Know-how. *Int J Biol Macromol* **2021**, *186*, 656-685, <https://doi.org/10.1016/j.ijbiomac.2021.07.067>.
31. Mallakpour, S.; Azadi, E.; Hussain, C.M. Chitosan, alginate, hyaluronic acid, gums, and β -glucan as potent adjuvants and vaccine delivery systems for viral threats including SARS-CoV-2: *Int J Biol Macromol* **2021**, *182*, 1931-1940, <https://doi.org/10.1016/j.ijbiomac.2021.05.155>.

32. Nelson, D.W.; Gilbert, R.J. Extracellular Matrix-Mimetic Hydrogels for Treating Neural Tissue Injury: A Focus on Fibrin, Hyaluronic Acid, and Elastin-Like Polypeptide Hydrogels. *Adv Healthc Mater* **2021**, *10*, 2101329, <https://doi.org/10.1002/adhm.202101329>.
33. Zhai, P.; Peng, X.; Li, B.; Liu, Y.; Sun, H.; Li, X. The application of hyaluronic acid in bone regeneration. *Int J Biol Macromol* **2020**, *151*, 1224-1239, <https://doi.org/10.1016/j.ijbiomac.2019.10.169>.
34. Abatangelo, G.; Vindigni, V.; Avruscio, G.; Pandis, L.; Brun, P. Hyaluronic Acid: Redefining Its Role. *Cells* **2020**, *9*, 1743, <https://doi.org/10.3390/cells9071743>.
35. Nascimento, L.D.; Nicoletti, N.F.; Peletti-Figueiró, M.; Marinowic, D.; Falavigna, A. Hyaluronic Acid In Vitro Response: Viability and Proliferation Profile of Human Chondrocytes in 3D-Based culture. *Cartilage* **2021**, *13*, 1077S-1087S, <https://doi.org/10.1177/19476035211057244>.
36. Ouasti, S.; Faroni, A.; Kingham, P.J.; Ghibaudi, M.; Reid, A.J.; Tirelli, N. Hyaluronic Acid (HA) Receptors and the Motility of Schwann Cell(-Like) Phenotypes. *Cells* **2020**, *9*, 1477, <https://doi.org/10.3390/cells9061477>.
37. Caon, I.; Bartolini, B.; Parnigoni, A.; Caravà, E.; Moretto, P.; Viola, M.; Karousou, E.; Vigetti, D.; Passi, A. Revisiting the hallmarks of cancer: The role of hyaluronan. *Semin Cancer Biol* **2020**, *62*, 9-19, <https://doi.org/10.1016/j.semcancer.2019.07.007>.
38. Silvestro, I.; Lopreiato, M.; Scotto, d'Abusco A.; Di Lisio, V.; Martinelli, A.; Piozzi, A.; Francolini, I. Hyaluronic Acid Reduces Bacterial Fouling and Promotes Fibroblasts' Adhesion onto Chitosan 2D-Wound Dressings. *Int J Mol Sci* **2020**, *21*, 2070, <https://doi.org/10.3390/ijms21062070>.
39. Amorim, S.; Pashkuleva, I.; Reis, C.A.; Reis, R.L.; Pires, R.A. Tunable layer-by-layer films containing hyaluronic acid and their interactions with CD44. *J Mater Chem B* **2020**, *8*, 3880-3885, <https://doi.org/10.1039/D0TB00407C>.
40. Soleymani, M.; Velashjerdi, M.; Shaterabadi, Z.; Barati, A. One-pot preparation of hyaluronic acid-coated iron oxide nanoparticles for magnetic hyperthermia therapy and targeting CD44-overexpressing cancer cells. *Carbohydr Polym* **2020**, *237*, 116130, <https://doi.org/10.1016/j.carbpol.2020.116130>.
41. Cheng, X.B.; Wang, S.; Yang, H.; Tong, H.; Shi, G.; Wu, L.; Zhou, J.; Shi, L.; Li, H.; Ren, S.; Zhou, Y.; Sato, N.; Zhou, J. Negative regulation between the expression levels of receptor for hyaluronic acid-mediated motility and hyaluronan leads to cell migration in pancreatic cancer. *Oncol Lett* **2020**, *20*, 199, <https://doi.org/10.3892/ol.2020.12060>.
42. Akentieva, N.; Topunov, A. RHAMM-Target Peptides as Molecular Imaging Probes for the Imaging of RHAMM-Expressing Cancer Cells. *Biointerface Research in Applied Chemistry* **2021**, *12*, 2-24, <https://doi.org/10.33263/BRIAC121.002024>.
43. Valachová, K.; Šoltés, L. Versatile Use of Chitosan and Hyaluronan in Medicine. *Molecules* **2021**, *26*, 1195, <https://doi.org/10.3390/molecules26041195>.
44. Akentieva, N.; Topunov, A. RHAMM-target peptides inhibit proliferation and viability of cancer cells. *Biointerface Research in Applied Chemistry* **2021**, *11*, 12252-12266, <http://dx.doi.org/10.33263/BRIAC114.1225212266>.
45. Carvalho, A.M.; Soares da Costa, D.; Paulo, P.M.R.; Reis, R.L.; Pashkuleva, I. Co-localization and crosstalk between CD44 and RHAMM depend on hyaluronan presentation. *Acta Biomater* **2021**, *119*, 114-124, <https://doi.org/10.1016/j.actbio.2020.10.024>.
46. Thangavel, C.; Boopathi, E.; Liu, Y.; Haber, A.; Ertel, A.; Bhardwaj, A.; Addya, S.; Williams, N.; Ciment, S.J.; Cotzia, P.; Dean, J.L.; Snook, A.; McNair, C.; Price, M.; Hernandez, J.R.; Zhao, S.G.; Birbe, R.; McCarthy, J.B.; Turley, E.A.; Pienta, K.J.; Feng, F.Y.; Dicker, A.P.; Knudsen, K.E.; Den, R.B. RB Loss Promotes Prostate Cancer Metastasis. *Cancer Res* **2017**, *77*, 982-995, <https://doi.org/10.1158%2F0008-5472.CAN-16-1589>.
47. Geskovski, N.; Matevska-Geshkovska, N.; Dimchevska Sazdovska, S.; Glavas Dodov, M.; Mladenovska, K.; Goracinova, K. The impact of molecular tumor profiling on the design strategies for targeting myeloid leukemia and EGFR/CD44-positive solid tumors. *Beilstein J Nanotechnol* **2021**, *12*, 375-401, <https://doi.org/10.3762/bjnano.12.31>.
48. Shi, R.; Liu, X. CD44: a potential therapeutic target in chronic myeloid leukemia. *Pharmazie* **2021**, *76*, 574-578, <https://doi.org/10.1691/ph.2021.1744>.
49. Klarić, M.; Haller, H.; Brnčić Fischer, A.; Babarović, E.; Prijčić, A.; Eminović, S. The Role of CD44 and RHAMM in Endometrial (Endometrioid Type) Cancer: An Immunohistochemical Study. *Appl Immunohistochem Mol Morphol* **2019**, *27*, 606-612, <https://doi.org/10.1097/pai.0000000000000673>.
50. Bychkova, V.E.; Basova, L.V.; Balobanov, V.A. How membrane surface affects protein structure.

- Biochemistry (Mosc)* **2014**, *79*, 1483-514, <https://doi.org/10.1134/S0006297914130045>.
51. Dobrzyńska, I.; Szachowicz-Petelska, B.; Darewicz, B.; Figaszewski, Z.A. Characterization of human bladder cell membrane during cancer transformation. *J Membr Biol* **2015**, *248*, 301-307, <https://doi.org/10.1007/s00232-015-9770-4>.
 52. Savchuk, O.A.; Silvestre, O.F.; Adão, R.M.R.; Nieder, J.B. GFP fluorescence peak fraction analysis based nanothermometer for the assessment of exothermal mitochondria activity in live cells. *Sci Rep* **2019**, *9*, 7535, <https://doi.org/10.1038/s41598-019-44023-7>.
 53. Faria, A.; Silvestre, O.F.; Maibohm, C.; Adão, R. M. R.; Silva, B.; Nieder, J. B. Cubosome nanoparticles for enhanced delivery of mitochondria anti-cancer drug elesclomol and therapeutic monitoring via sub-cellular NAD(P)H multi-photon fluorescence lifetime imaging. *Nano Research* **2019**, *12*, 991-998, <https://doi.org/10.1007/s12274-018-2231-5>.
 54. Wang, Z.H.; Tian, Y.F.; Zhang, H.; Qin, Y.M.; Li, D.; Gan, L.; Wu, F.H. Using hyaluronic acid-functionalized pH stimuli-responsive mesoporous silica nanoparticles for targeted delivery to CD44-overexpressing cancer cells. *Int J Nanomedicine* **2016**, *11*, 6485-6497, <https://doi.org/10.2147/IJN.S117184>.
 55. Piperigkou, Z.; Kyriakopoulou, K.; Koutsakis, C.; Mastronikolis, S.; Karamanos, N.K. Key Matrix Remodeling Enzymes: Functions and Targeting in Cancer. *Cancers (Basel)* **2021**, *13*, 1441, <https://doi.org/10.3390/cancers13061441>.
 56. Du, K.; Xia, Q.; Heng, H.; Feng, F. Temozolomide-Doxorubicin Conjugate as a Double Intercalating Agent and Delivery by Apoferritin for Glioblastoma Chemotherapy. *ACS Appl Mater Interfaces* **2020**, *12*, 34599-34609, <https://doi.org/10.1021/acsami.0c08531>.
 57. Mazurek, M.; Rola, R. The implications of nitric oxide metabolism in the treatment of glial tumors. *Neurochem Int* **2021**, *150*, 105172, <https://doi.org/10.1016/j.neuint.2021.105172>.
 58. Alimoradi, H.; Greish, K.; Gamble, A.B.; Giles, G.I. Controlled Delivery of Nitric Oxide for Cancer Therapy. *Pharm Nanotechnol* **2019**, *7*, 279-303, <http://dx.doi.org/10.2174/2211738507666190429111306>.
 59. Soni, Y.; Softness, K.; Arora, H.; Ramasamy, R. The Yin Yang Role of Nitric Oxide in Prostate Cancer. *Am J Men's Health* **2020**, *14*, 1557988320903191, <https://doi.org/10.1177%2F1557988320903191>.
 60. Hu, Y.; Xiang, J.; Su, L.; Tang, X. The regulation of nitric oxide in tumor progression and therapy. *J Int Med Res* **2020**, *48*, 300060520905985, <https://doi.org/10.1177%2F0300060520905985>.
 61. Khan, F.H.; Dervan, E.; Bhattacharyya, D.D.; McAuliffe, J.D.; Miranda, K.M.; Glynn, S.A. The Role of Nitric Oxide in Cancer: Master Regulator or NOT? *Int J Mol Sci* **2020**, *21*, 9393, <https://doi.org/10.3390/ijms21249393>.
 62. Ji, X.; Chen, Q.; Arutla, V.; Khdour, O.; Hu, Q.Y.; Chen, S. Double-component diazeniumdiolate derivatives as anti-cancer agents. *Bioorg Med Chem* **2020**, *28*, 115405, <https://doi.org/10.1016/j.bmc.2020.115405>.
 63. Kang, F.; Ai, Y.; Zhang, Y.; Huang, Z. Design and synthesis of new hybrids from 2-cyano-3,12-dioxooleana-9-dien-28-oic acid and O²-(2,4-dinitrophenyl) diazeniumdiolate for intervention of drug-resistant lung cancer. *Eur J Med Chem* **2018**, *149*, 269-280, <https://doi.org/10.1016/j.ejmech.2018.02.062>.
 64. Zou, Y.; Yan, C.; Liu, J.C.; Huang, Z.J.; Xu, J.Y.; Zhou, J.P.; Zhang, H.B.; Zhang, Y.H. Synthesis and anti-hepatocellular carcinoma activity of novel O²-vinyl diazeniumdiolate-based nitric oxide-releasing derivatives of oleanolic acid. *Chin J Nat Med* **2017**, *15*, 928-937, [https://doi.org/10.1016/S1875-5364\(18\)30009-8](https://doi.org/10.1016/S1875-5364(18)30009-8).
 65. Basudhar, D.; Cheng, R.C.; Bharadwaj, G.; Ridnour, L.A.; Wink, D.A.; Miranda, K.M. Chemotherapeutic potential of diazeniumdiolate-based aspirin prodrugs in breast cancer. *Free Radic Biol Med* **2015**, *83*, 101-114, <https://doi.org/10.1016/j.freeradbiomed.2015.01.029>.
 66. Jin, H.; Feura, E.S.; Schoenfisch, M.H. Theranostic Activity of Nitric Oxide-Releasing Carbon Quantum Dots. *Bioconjug Chem* **2021**, *32*, 367-375, <https://doi.org/10.1021/acs.bioconjchem.1c00002>.
 67. Fu, J.; Liu, L.; Huang, Z.; Lai, Y.; Ji, H.; Peng, S.; Tian, J.; Zhang, Y. Hybrid molecule from O²-(2,4-dinitrophenyl)diazeniumdiolate and oleanolic acid: a glutathione S-transferase π -activated nitric oxide prodrug with selective anti-human hepatocellular carcinoma activity and improved stability. *J Med Chem* **2013**, *56*, 4641-4655, <https://doi.org/10.1021/jm400393u>.
 68. Sun, T.; Lv, T.; Wu, J.; Zhu, M.; Fei, Y.; Zhu, J.; Zhang, Y.; Huang, Z. General Strategy for Integrated Bioorthogonal Prodrugs: Pt(II)-Triggered Depropargylation Enables Controllable Drug Activation In Vivo. *J Med Chem* **2020**, *63*, 13899-13912, <https://doi.org/10.1021/acs.jmedchem.0c01435>.
 69. Puglisi, M.P.; Bradaric, M.J.; Pontikis, J.; Cabai, J.; Weyna, T.; Tednes, P.; Schretzman, R.; Rickert, K.; Cao, Z.; Andrei, D. Novel primary amine diazeniumdiolates-Chemical and biological characterization. *Drug Dev Res* **2018**, *79*, 136-143, <https://doi.org/10.1002/ddr.21428>.

70. Akentieva, N.P.; Sanina, N.A.; Gizatullin, A.R.; Shmatko, N.Y.; Goryachev, N.S.; Shkondina, N.I.; Prihodchenko, T.R.; Aldoshin, S.M. The inhibitory effect of dinitrosyl iron complexes (NO donors) on myeloperoxidase activity. *Dokl Biochem Biophys* **2017**, *477*, 389-393, <https://doi.org/10.1134/S1607672917060126>.
71. Akentieva, N.P.; Sanina, N.A.; Prichodchenko, T.R.; Gizatullin, A.R.; Shkondina, N.I.; Shushanov, S.S.; Stupina, T.S.; Aldoshin, S.M. Anticancer Activity of Dinitrosyl Iron Complex (NO Donor) on the Multiple Myeloma Cells. *Dokl Biochem Biophys* **2019**, *486*, 238-242, <https://doi.org/10.1134/S1607672919030190>.
72. Akentieva, N.; Sanina, N.; Gizatullin, A.; Shkondina, N.; Andreeva, A.; Shram, S.; Aldoshin, S. Influence of Dinitrosyl Iron Complexes on the Activity of Enzymes, Indicators of Cardiovascular Diseases. *Biointerface Res Appl Chem* **2022**, *13*, 2, 2023, 198, <https://doi.org/10.33263/BRIAC132.198>.
73. Vanin, A.F.; Tronov, V.A.; Borodulin, R.R. Nitrosonium Cation as a Cytotoxic Component of Dinitrosyl Iron Complexes with Thiol-containing Ligands (based on the Experimental Work on MCF7 Human Breast Cancer Cell Culture). *Cell Biochem Biophys* **2021**, *79*, 93-102, <https://doi.org/10.1007/s12013-020-00962-x>.
74. Wu, S.C.; Lu, C.Y.; Chen, Y.L.; Lo, F.C.; Wang, T.Y.; Chen, Y.J.; Yuan, S.S.; Liaw, W.F.; Wang, Y.M. Water-Soluble Dinitrosyl Iron Complex (DNIC): a Nitric Oxide Vehicle Triggering Cancer Cell Death via Apoptosis. *Inorg Chem* **2016**, *55*, 9383-9392, <https://doi.org/10.1021/acs.inorgchem.6b01562>.
75. Liu, X.Y.; Wang, J.Q.; Ashby, C.R. Jr.; Zeng, L.; Fan, Y.F.; Chen, Z.S. Gold nanoparticles: synthesis, physicochemical properties and therapeutic applications in cancer. *Drug Discov Today* **2021**, *26*, 1284-1292, <https://doi.org/10.1016/j.drudis.2021.01.030>.
76. Farzin, A.; Etesami, S.A.; Quint, J.; Memic, A.; Tamayol, A. Magnetic Nanoparticles in Cancer Therapy and Diagnosis. *Adv Healthc Mater.* **2020**, *9*, e1901058, <https://doi.org/10.1002/adhm.201901058>.
77. Lee, K.; Kim, T.; Kim, Y.M.; Yang, K.; Choi, I.; Roh, Y.H. Multifunctional DNA Nanogels for Aptamer-Based Targeted Delivery and Stimuli-Triggered Release of Cancer Therapeutics. *Macromol Rapid Commun.* **2021**, *42*, 2000457, <https://doi.org/10.1002/marc.202000457>.
78. Li, X.; Jian, M.; Sun, Y.; Zhu, Q.; Wang, Z. The Peptide Functionalized Inorganic Nanoparticles for Cancer-Related Bioanalytical and Biomedical Applications. *Molecules* **2021**, *26*, 3228, <https://doi.org/10.3390/molecules26113228>.